Proceedings of Global Power and Propulsion Society
ISSN-Nr: 2504-4400
GPPS Hong Kong 2023
October 17-19, 2023
www.gpps.global

GPPS-TC-2023-0298

Meso-scale investigation on the deformation and failure behaviors of plain woven SiC/SiC with holes

Xin JING
School of Power and Energy, NWPU
Email: jingxin@nwpu.edu.cn
Xian, Shanxi, China

Fang ZENG
School of Power and Energy, NWPU
Email:zfang@mail.nwpu.edu.cn
Xian, Shanxi, China

ABSTRACT

For plain woven SiC/SiC composites used in the aerospace thermal-structural applications, not only the pristine material properties but the open-hole performance are of critical concern for the components in service. In the present study, the influence of fiber preform and manufactured hole on the macro mechanical properties of plain woven SiC/SiC were investigated experimentally. Tensile tests at room temperature were conducted on SiC/SiC specimens with different hole apertures and configurations, and digital image correlation (DIC) method was used for full field strain measurement. The results showed that mesoscopic deformation and failure of pristine SiC/SiC specimens during tensile loading were closely related to the mesoscopic structure of plain woven fabrics. The notch sensitivity of SiC/SiC strength is weak, and the local mesoscopic deformation of the notch is affected by the work of macroscopic stress gradients and mesoscopic structures.

INTRODUCTION

SiC/SiC composites are the key thermal-structural materials for hot-section components of current and future aero-engines, which exhibits lower density, high service temperature and lower thermal expansion compared to the current used superalloys. The usage of SiC/SiC will significantly increase the turbine front temperature of aircraft engines, thereby improving work efficiency and performance. Currently, the manufacture of SiC/SiC composites are mostly based on fiber tows (also known as mini-composites) which are composed of hundreds or thousands of fibers. The tows are woven or braided into preforms firstly, and then prepared through matrix densification processes such as CVI, PIP, or MI. Therefore, textile SiC/SiC exhibits a multi-scale structure of micro (fiber/interface/matrix) - meso (textile preform) - macro (SiC/SiC structure). Variations in micro/meso-scale constituents and geometries will change the macro mechanical properties, thereby affecting the structural strength design of components. In some applications such as turbine blades and combustion chambers, the components will inevitably contain geometric hole structures. which usually need to cooperate with cooling structures to introduce cooling airflow to reduce the working temperature of the structure. Due to the small size of the cooling holes, they were usually introduced by drilling on as-prepared composites panel after processing has been completed (like laser cutting), or by deflecting local fiber tows prior to matrix densification (like insertion of fugitive rods into the woven preform). In addition, it also includes typical hole structures with different sizes such as bolt connections (~5mm), hot/cold air mixing holes (10mm). Such discontinuities may introduce stress concentration around the hole edge, and finally lead to strength or life reduction of composite structures.

The relevant study on notch sensitivity has been undertaken previously for a wide range of Ceramic matrix composites (CMCs) such as C/C, oxide/oxide and SiC/SiC, concerning from room temperature notch strength [Mcnulty,2010; Haque, 2010], high temperature /environmental notch strength [Meyer, 2018; Hui, 2018], notch fatigue [Mcnulty, 2001; Ruggles, 2012], to notch creep [Wu, 2006]. The basic conclusion is that the notch sensitivity is related to the material system of CMCs. Due to their toughening mechanism and pseudo-plastic characteristics, C/SiC and SiC/SiC with SiC matrix exhibit relatively weak notch sensitivity through stress redistribution at the notch tip to reduce the stress concentration, and exhibit a certain size effect. However, the early studies did not consider the role of textile structures. On the one hand, the geometric discontinuity introduced by the hole will generate a stress gradient near the notch. On the other hand, the heterogeneous periodic textile structure of composite materials will generate local strain fluctuations. The coupling effect of heterogeneous deformation and notch stress gradient results in complex elastic/inelastic deformation and damage evolution in the local portion of the notch, and becomes more apparent when the geometric size of the notch is similar to the size of the cellular fiber bundle. The strain gauge measurement method cannot further study such detailed strain field distribution at the notch, especially the influence of the microstructure of the fiber bundle.

In recent years, DIC technology has been widely used in the experimental measurement of the mesoscopic deformation field of composite materials [Blacklock, 2016; Teng, 2019] and the notch strain field [Meyer, 2018; Gao, 2017]. For example, Meyer and Gao Xiguang have respectively analyzed the notch strain of laminated SiC/SiC and needled C/SiC, obtaining the hole edge strain field and crack propagation path. However, in the above study, the local strain field analysis with a larger pore diameter and a stronger interaction between the pore periphery and the heterogeneous meso-structure is not involved, and the initial deformation and damage mechanisms that affect the failure of the small hole are not clear.Mei [Mei, 2016] considered a small hole with a diameter of 0.5mm in the notch strength study of two-dimensional plain grain C/SiC. When the pore diameter decreases from 3mm to 0.5mm, the tensile strength increases, especially the strength retention rate of 0.5mm pores is above 90%. Zhang [Zhang, 2020] tested the tensile strength of three-dimensional braided SiC/SiC with a diameter of 0.5 mm and found that the tensile strength of single and row holes decreased by 6% and 8%, respectively. Mei further studied the C/SiC bending strength of rows of holes. For rows of holes with an aperture of 0.5 mm and a spacing of 2 mm, the room temperature strength retention rate is above 90%. The location information of the openings was statistically analyzed whether they were located at the junction of the fiber bundle, matrix, or both, but no correlation analysis was performed between the location differences and strength data. None of the above work has investigated the strain field at the notch and its impact on notch failure. As a preliminary attempt to study the strain field around a small hole, Shaw [Shaw, 2015] conducted a strength test on a three-dimensional woven C/SiC with an diameter of 1 mm. The strain field measured by DIC indicates that the deformation field around the hole is affected by a combination of periodic cell structure and stress concentration around the hole. For flat specimens, the strain exhibits a periodic distribution, and when the load increases, nonlinear deformation occurs, corresponding to the opening of finite transverse cracks within the cell, The crack location is related to the periodic meso-structure; Due to the strain concentration around the hole, the impact distance on the local strain field of the sample with holes reaches 1-1.5 cells. The density of cracks around the hole is higher and the stress concentration intensifies the generation and propagation of longitudinal, transverse, and shear cracks around the hole.

Specifically, the main purpose of the present work is to investigate the effect of fabric and holes on the tensile performance and failure mechanisms of a plain woven SiC/SiC by experimental methods. The tensile behavior of unnotched and notched specimens were experimental characterized, and the full-field strain maps were recorded using DIC. Especially, the convolution effects of competing size scales—notably, those of the hole and the woven structure —are discussed.

MATERIAL AND EXPERIMENTAL DETAILS

Materials and specimens

The SiC/SiC composites in this study were provided by the Thermo-structural Composite Materials Laboratory (TCML), NWPU. The plain woven cloths of 1K Cansas-II SiC fibers were fabricated into a ten layer laminated architecture, and fiber volume fraction was approximately 40%. The preform was then surrendered to a chemical vapor deposition (CVD) process to deposit an pyrolytic carbon (PyC) layer. Following this, the SiC matrix were infiltrated into the fiber preform by Chemical vapor infiltration (CVI). The SiC/SiC composites were machined into dog-bone shaped tensile specimens along warp direction (as shown in Fig. 1). The overall specimen dimensions were roughly 120 mm×12 mm×3mm and the central gage section were 30 mm×10mm×3 mm.

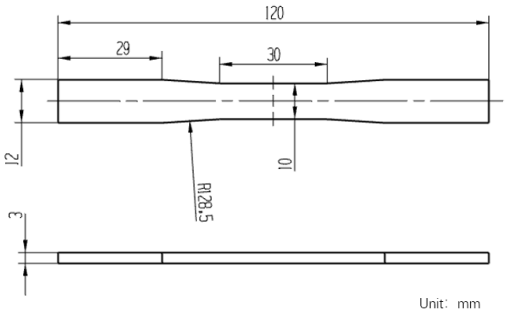

Figure 1 SiC/SiC specimen

In order to study the hole induced mechanical reduction of SiC/SiC, 3 hole configurations were machined on the tensile specimens. In first two of them the single hole with diameter of 0.5mm and 2mm was situated at the center of the gauge section. The last one contained four holes which were the four corner points of a square. The hole diameter was 0.5mm and the distance was 2mm. All the holes were machined/drilled by laser method.

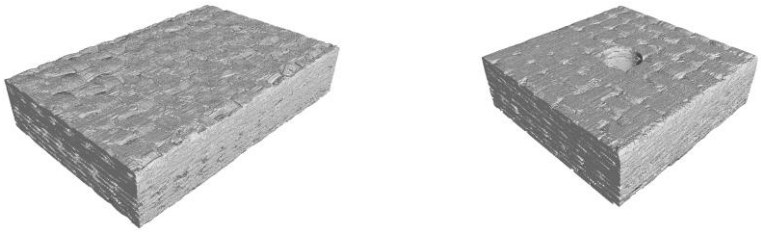

Figure 2 Microstructure of (a) pristine and (b) 2mm-hole specimens.

Materials and specimens

The static tensile tests were conducted on a servo-hydraulic test machine (Instron 8802). The tensile process was under a displacement control mode at a rate of 0.3mm/min (nominal strain rate of 4×10-5 s-1) to simulate the quasi-static loading process. Prior to experiment, each specimen was painted black first and a white speckle pattern was then created using an airbrush. The regions probed by DIC were 10 mm long and encompassed the full specimen width, The length of the region of interest represents more than three times the unit cell length in both warp and weft directions. During test, 1Hz sampling frequency was adopted to obtain the images. After test, the displacement and strain were calculated using a subset size of 21pixels and a step size of 3pixels.

To verify the accuracy of DIC, a contact type extensometer (Instron2630-101) was fixed at the gage section for some specimens to directly measure the macro strain. The results were shown in fig.3. It could be seen that the DIC result correlated well with the extensometer result, except a slight discrepancy before failure. As the extensometer may interference field of view to reduce the effective measure area, most of macro strain were measured by DIC. The DIC data were then used to characterize local deformation patterns associated with the holes and the fiber architecture in following 2 forms: (1) as full-field strain maps over the entire correlated area, (2) as line scans of axial displacement with axial positions. As the underlying fiber tows could be discerned, the tow boundaries were subsequently superimposed on some strain maps.

RESULTS AND DISCUSSION

Mechanical behaivors of SiC/SiC without holes

The typical tensile stress-strain responses of the pristine specimens of plain woven SiC/SiC composites are shown in Fig.3. Although there were little discrepancies of each sample, all curves exhibit a same multi-stage evolution and non-brittle failure feature, with a linear domain (stage I) having an elastic modulus of about 160 GPa. The curves were linear up to about 75MPa (0.06% strain) and the nonlinearity was significant in the range 75-125MPa (Stage II) , similar to the yield behavior of metal plasticity. After that, the response was again approximately linear (Stage III), with a tangent modulus of about 30 GPa. By comparison, the modulus calculated on the basis of the volume fraction of warp tows (assumed to be straight) and the reported modulus of SiC fibers (E_f = 210 GPa) is $f_{warp}E_f$ = 42 GPa (f_{warp} was set to 0.2 as equal fiber volume fraction in warp and weft directions), which was higher than the measured tangent modulus. The difference suggested that the matrix attained a nearly fully damaged state and the undulating warp tows also undergo some progressive damage. At last, when the strain is about 0.4%, the material enters the nonlinear failure stage (stage IV), where the material stiffness gradually decreases until complete fracture failure occurs. The variation in each specimen became visible, especially in the final tensile strength and fracture strain. The average strength of the three specimens is about 246MPa. The corresponding transverse strain under tensile load is also shown in Fig. e, primarily caused by transverse shrinkage due to the Poisson effect. The negative transverse strain intensifies as the load increases, particularly when the material is close to failure. This indicates that significant damage relevant to transverse deformation may occur at the beginning of the fourth stage.

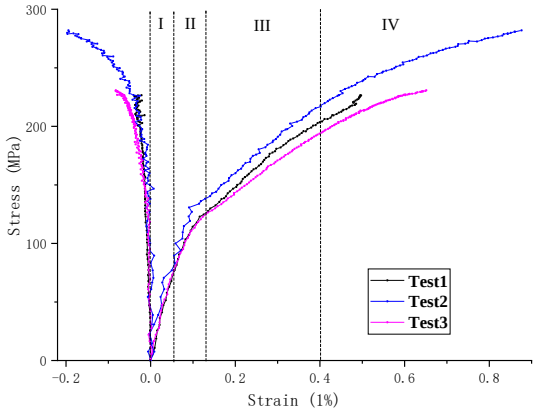

Figure 3 Tensile stress-strain curve of SiC/SiC specimens without hole

Full-field map of longitudinal strain at different macroscopic stresses are shown in Fig.4. The white dotted lines in the figure indicate the corresponding positions of warp and weft yarns on the surface of the sample. The strain fields exhibit distinct periodic patterns during whole loading process. Fig.4 (a-c) shows the strain field at a macroscopic stress of 48, 75, and 125 MPa, respectively, corresponding to the I-III stage in the tensile curve. In elastic domain (48 MPa), the surface of the sample exhibits periodic fluctuations in high and low strain. The low strain region was warp yarn, and the high strain region is weft yarn. Besides, there is a high strain band between the adjacent rows/columns of weft yarns, forming a prototype of strain bands that are approximately fishnet shaped in distribution. As the load increases (75 MPa), the strain concentration further intensified at the upper and lower edges of the weft yarn. These strain concentration bands were wavy, with the wave crest facing the inner centerline of the weft yarn. An X-shaped pattern was formed in the same weft yarn, while adjacent rows of weft yarns are connected to each other in a wavy pattern, resulting in a diamond-shaped strain concentration pattern in the entire strain field. As the stress increases further (125 MPa), the wavy strain concentration bands continue to converge, eventually converging to the upper and lower edges of the weft yarn, and the upper and lower bands in the same weft yarn were separated. They are characterized by narrow bands of high apparent strain (well over 1%) and intervening regions with negligible strain. Shaw pointed out that these narrow bands are attributed to the opening of matrix cracks. The displacement discontinuity at each crack appears in the DIC data as a near-linear variation in displacement. Figure c-f shows that with the further increase of load, the number and position of strain bands no longer change, but the strain values in the bands increase dramatically with different intensification rates of different bands are different. Some bands experiencing increased strain concentration, while others experiencing a slowdown that is almost unrecognizable. This means that cracks have formed and gradually expanded at these former locations. As can be seen in the figure, an obvious crack has formed in the upper and lower regions of the specimen. At this time, some areas with large cracks on the specimen surface cannot calculate the strain due to the discontinuity of the material. These cracks gradually extend transversely to the entire specimen width, and eventually the crack in the upper left corner becomes the main crack, leading to the final complete fracture of the specimen (Figure f).

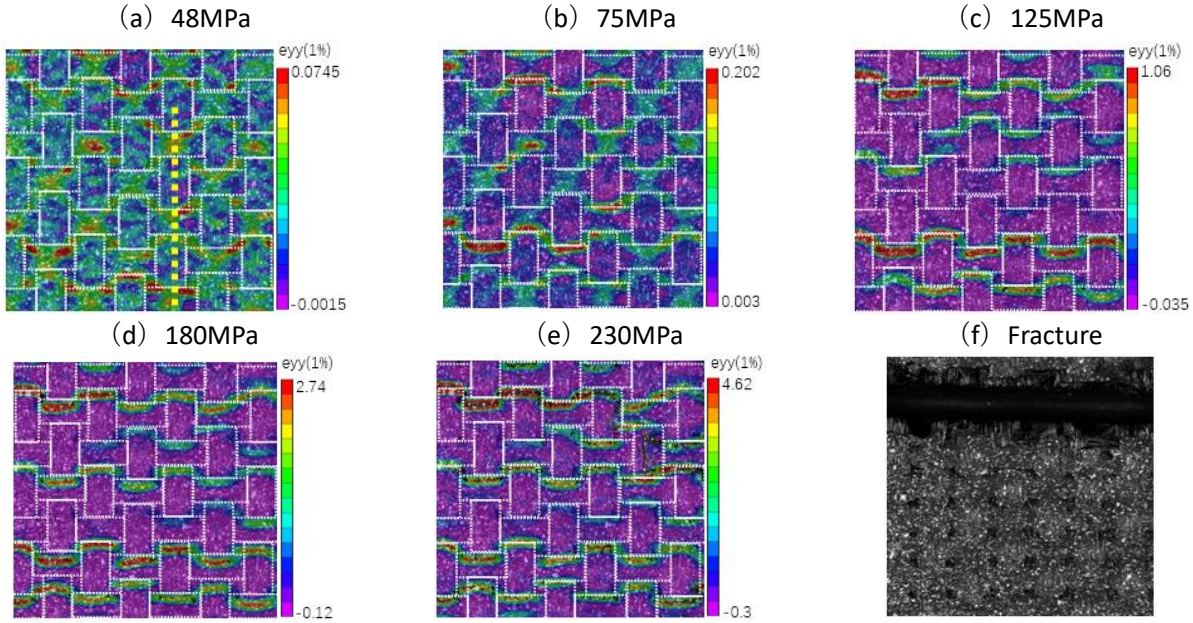

Figure 4 Longitudinal strain field of plain woven SiC/SiC under different stress levels

The strain band is more prominent in line scan of axial strains, shown in Fig.5. The scanned line is shown in Fig.4 and spans two warp and weft yarns, with a length of 6.6 mm. It can be seen that at the initial elastic stage, both the warp and weft surface strains exhibit certain fluctuations, and the weft strain is larger than the warp, but the magnitude of the two is consistent, which is related to the initial non-uniform elastic strain field caused by the material's woven structure and the fluctuation of the material's surface morphology. As the load increases and enters the inelastic stage, the edge strain of the weft yarn rapidly increases, forming an obvious peak strain, indicating that cracks appear in these areas. As the load continues to increase, the number and location of cracks no longer change, while the peak strain at the crack continues to increase. The rest regions between each bands exhibits almost constant strain as the displacement changes from one level to another at each crack band. The growth of surface cracks on the specimen is not synchronous, with some cracks propagating rapidly and some cracks propagating slowly. For example, when the stress is 75 MPa, an obvious wave peak has appeared at about 3.3 mm. As the stress increases to 125 MPa, the wave peak here has almost no change. Although it continues to increase later, the overall strain value is still smaller than other cracks.

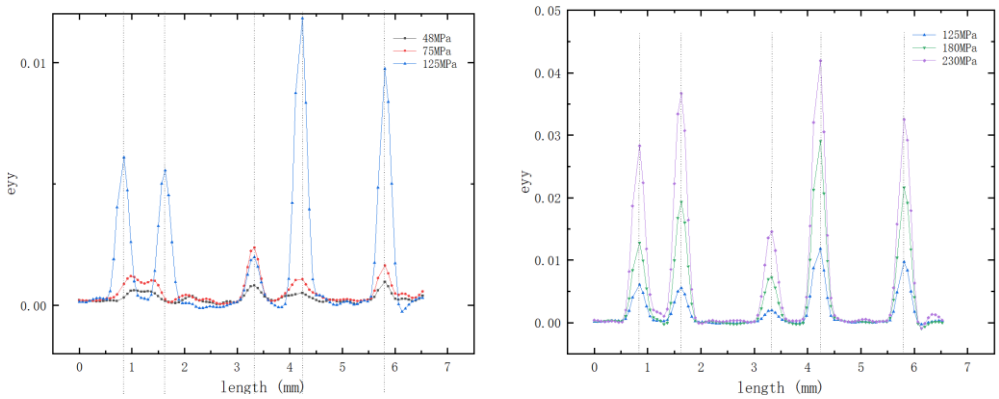

Figure 5 Evolution law of surface cracks in plain weave SiC/SiC

Mechanical behaivors of SiC/SiC with holes

The tensile stress-strain curves for specimens containing holes are plotted in Fig.6a in terms of the remote stress, which appear to collapse onto the curves for unnotched specimens except the final failure. Variation in UTS with hole size are plotted in Fig.6b and the result exhibited a significant weak sensitivity. The slight strength reductions associated with the holes can be rationalized to mainly on the basis of the reduced net-section area. The nominal macroscopic strength of the 0.5 mm single hole specimen is 234 MPa, and the net cross-sectional stress of the notch is 246 MPa, which is almost identical to that of the non hole specimen. The nominal macroscopic strength of a 2mm single hole specimen is 226MPa, which is approximately 92% of that of a flat plate specimen. The strength of the 0.5 mm four hole specimen of SiC/SiC is about 212 MPa, which is about 14% lower than that of the non hole specimen. This shows that two holes with relatively close distances have a strong interaction, leading to a significant reduction in strength.

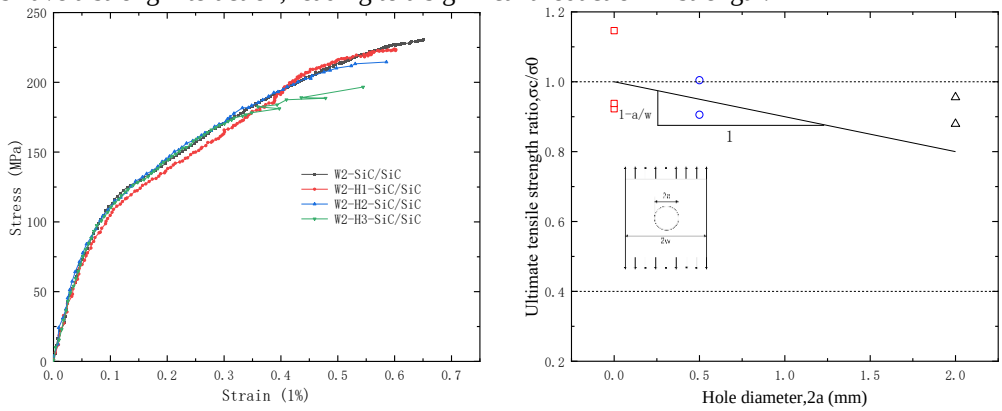

Figure 6 Tensile stress-strain curve of plain weave SiC/SiC with holes

Full field longitudinal strain maps for these specimens are shown in Fig.7, at remote stress levels corresponding to the linear elasticity, nonlinear damage, and about to fail. The strain fields were again characterized by initial periodic diamond shaped and following banded patterns reflecting the weave geometry and relevant cracks. The location and spacing of high strain bands were the same with the unnotched specimens, indicating the weave structure still plays an important role in the deformation and damage state during loading process. On the other hand, the dependence of holes on the evolution of patterns appeared at higher stress. As the holes behaved as stress concentrators, the strain bands expanded more intensely adjacent transversely to the holes and diminished to the value comparable to the pristine specimens in regions remote from the holes. For example, for the 0.5 mm single hole sample in Fig 7, the hole position was inside the yarn. When the load is relatively small, the strain field mainly displays a correlation with the characteristics of the woven structure. There are equidistant discontinuous strain concentration bands (121 MPa) distributed on the surface of the sample. When the stress increases to 180 MPa, there are one microcrack on the upper left side and one microcrack on the right side of the hole that expands rapidly, and the two adjacent microcracks on the upper and lower sides gradually connect together, A crack across the surface of the specimen was formed, resulting in the final fracture of the specimen. The strain distribution in the hole edge region of a 2mm single hole sample does not exhibit an obvious periodic pattern. When the load is 121 MPa, due to the stress concentration at the hole edge, a microcrack initiates on both sides of the hole, and rapidly expands to the edge of the sample as the stress increases. The opening position of the 0.5mm four-hole sample is at the edge of the weft yarn. During the loading process, there is a microcrack propagation at the upper and lower two hole positions. As the stress increases, the microcrack propagation at the lower two hole positions is faster, leading to the final fracture of the sample.

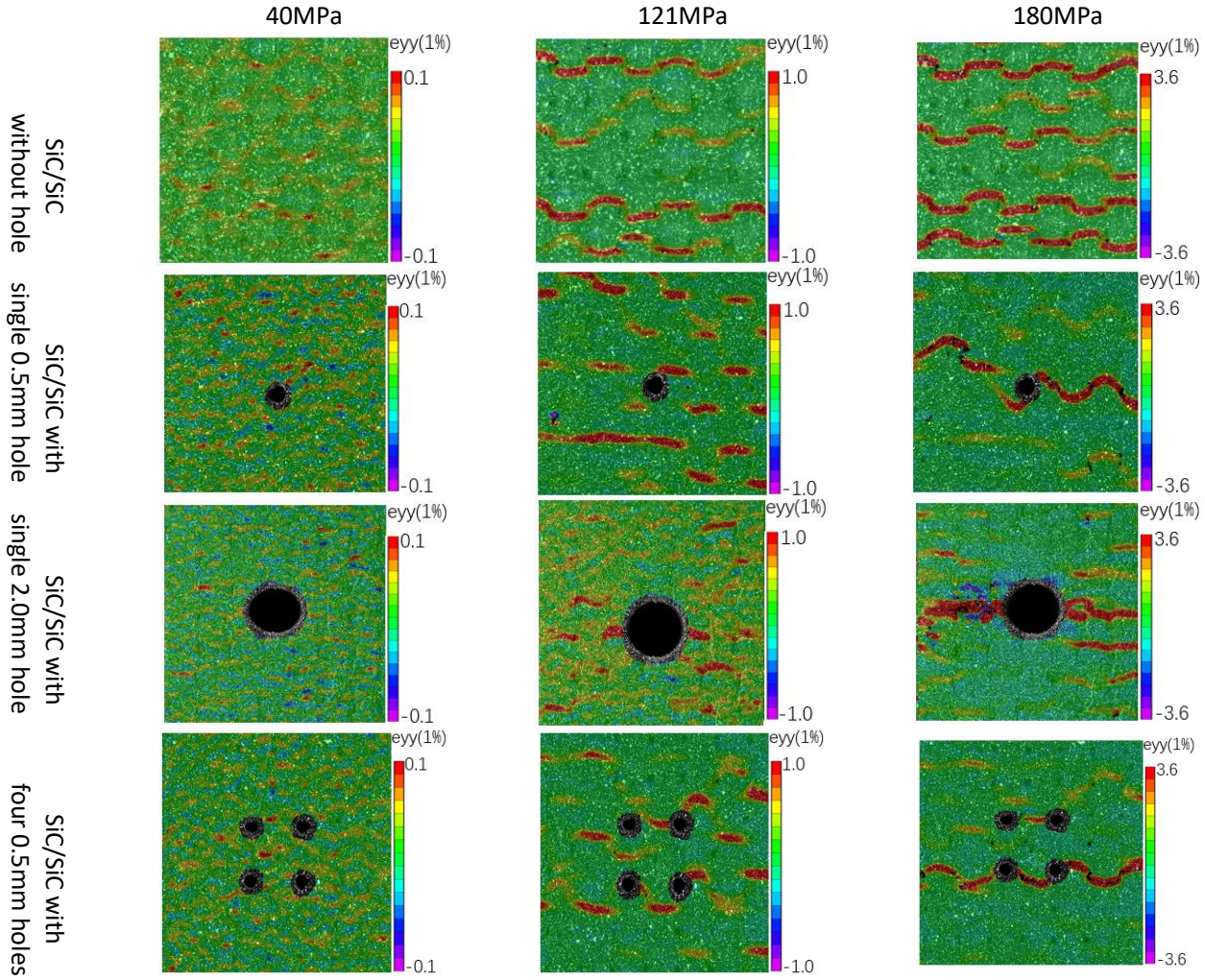

Figure 7 Longitudinal strain field of plain woven SiC/SiC with holes

CONCLUSIONS

The influence of fiber fabric and manufactured hole on the macro mechanical properties of plain woven SiC/SiC were experimentally investigated. The main conclusions are listed belows:

(1) The deformation and failure behaviors of plain woven SiC/SiC flat specimens are highly influenced by the meso-scale structrues. Periodic strain patterns were measured and the high strain bands were located in the intersection of warp and weft yarns. These bands were micro cracks which open more severe as stress increase, and lead to ultimate fracture.

(2) The notch strength sensitivity of plain woven SiC/SiC materials is weak. The high strain bands were still observed in the notched specimens, but the damge evolution was more severer due to the stress concentration. The ultimate failures were highly correlated to fabric structures when the diameter is 0.5mm.

ACKNOWLEDGMENTS

The research was supported by National Natural Science Foundation of China (NSFC51802264), the Natural Science Foundation of Shaanxi Province (2020JQ-177) and the Fundamental Research Funds for the Central Universities (31020190MS705).

References

Blacklock, M. , Shaw, J. H. , Zok, F. W. , & Cox, B. N. . (2016). Virtual specimens for analyzing strain distributions in textile ceramic composites. *Composites Part A: Applied Science and Manufacturing*.

Gao, X. , Yu, G. , Xue, J. , & Song, Y. . (2017). Failure analysis of c/sic composites plate with a hole by the pfa and dic method. *Ceramics International, 43*(6), 5255-5266.

Haque, A. , Ahmed, L. , & Ramasetty, A. . (2010). Stress concentrations and notch sensitivity in woven ceramic matrix composites containing a circular hole—an experimental, analytical, and finite element study. *Journal of the American Ceramic Society, 88*(8), 2195-2201.

Hui, M. , Chen, T. , Ding, Z. , & Cheng, L. . (2018). Oxidation degradation and mechanical reduction on c/sic composites with artificial notch defects. *Ceramics International, 44*(12), 13873-13878.

Mcnulty, J. C. , He, M. Y. , & Zok, F. W. . (2001). Notch sensitivity of fatigue life in a sylramic tm/sic composite at elevated temperature. *Composites Science & Technology, 61*(9), 1331-1338.

Mcnulty, J. C. , Zok, F. W. , Genin, G. M. , & Evans, A. G. . (2010). Notch-sensitivity of fiber-reinforced ceramic-matrix composites: effects of inelastic straining and volume-dependent strength. *Journal of the American Ceramic Society, 82*(5), 1217-1228.

Mei, H. , Zhang, D. , Xia, J. , Yu, C. , & Cheng, L. . (2016). The effect of hole defects on the oxidation behaviour of two-dimensional c/sic composites. *Ceramics International*, 15479-15484.

Meyer, P. , & Waas, A. M. . (2018). Experimental results on the elevated temperature tensile response of sic/sic ceramic matrix notched composites. *Composites Part B Engineering, 143*(JUN.), 269-281.

Ruggles-Wrenn, M. B. , Delapasse, J. , Chamberlain, A. L. , Lane, J. E. , & Cook, T. S. . (2012). Fatigue behavior of a hi-nicalon/sic–b4c composite at 1200 °c in air and in steam. *Materials Science & Engineering A, 534*(Feb.1), 119-128.

Shaw, J. H. , Rossol, M. N. , Marshall, D. B. , Zok, F. W. , & Cinibulk, M. . (2015). Effects of tow-scale holes on the mechanical performance of a 3d woven c/sic composite. *Journal of the American Ceramic Society, 98*(3), 948-956.

Teng, X. , Shi, D. , Cheng, Z. , Jing, X. , & Yang, X. . (2019). Investigation on non-uniform strains of a 2.5d woven ceramic matrix composite under in-plane tensile stress. *Journal of the European Ceramic Society, 40*(1).

Wu, X. , Qiao, S. , Hou, J. , Zhao, Q. , & Mei, L. . (2006). Tensile creep behavior of notched two-dimensional-c/sic composite. *Composites Science and Technology, 66*(7), 993-1000.

Zhang, X. H. , Gao, H. S. , Wen, Z. X. , Li, M. Y. , Zhou, X. G. , & Yue, Z. F. . (2020). Tension-tension fatigue behaviour of 3d braided sicf/sic composite with film cooling holes at 1350 degrees c in air. *Ceramics International*,(6), 46.